An ^{18}F-FDG PET/CT and Mean Lung Dose Model to Predict Early Radiation Pneumonitis in Stage III Non–Small Cell Lung Cancer Patients Treated with Chemoradiation and Immunotherapy

Maria Thor[1], Chen Lee[1], Lian Sun[1], Purvi Patel[1], Aditya Apte[1], Milan Grkovski[1], Annemarie F. Shepherd[2], Daphna Y. Gelblum[2], Abraham J. Wu[2], Charles B. Simone II[2], Jamie E. Chaft[3], Andreas Rimner[2], Daniel R. Gomez[2], Joseph O. Deasy[1], and Narek Shaverdian[2]

[1]Department of Medical Physics, Memorial Sloan Kettering Cancer Center, New York, New York; [2]Department of Radiation Oncology, Memorial Sloan Kettering Cancer Center, New York, New York; and [3]Thoracic Oncology Service, Memorial Sloan Kettering Cancer Center, New York, New York

Radiation pneumonitis (RP) that develops early (i.e., within 3 mo) (RP$_{Early}$) after completion of concurrent chemoradiation (cCRT) leads to treatment discontinuation and poorer survival for patients with stage III non–small cell lung cancer. Since no RP$_{Early}$ risk model exists, we explored whether published RP models and pretreatment ^{18}F-FDG PET/CT–derived features predict RP$_{Early}$. **Methods:** One hundred sixty patients with stage III non–small cell lung cancer treated with cCRT and consolidative immunotherapy were analyzed for RP$_{Early}$. Three published RP models that included the mean lung dose (MLD) and patient characteristics were examined. Pretreatment ^{18}F-FDG PET/CT normal-lung SUV featured included the following: 10th percentile of SUV (SUV$_{P10}$), 90th percentile of SUV (SUV$_{P90}$), SUV$_{max}$, SUV$_{mean}$, minimum SUV, and SD. Associations between models/features and RP$_{Early}$ were assessed using area under the receiver-operating characteristic curve (AUC), P values, and the Hosmer–Lemeshow test (pHL). The cohort was randomly split, with similar RP$_{Early}$ rates, into a 70%/30% derivation/internal validation subset. **Results:** Twenty (13%) patients developed RP$_{Early}$. Predictors for RP$_{Early}$ were MLD alone (AUC, 0.72; $P = 0.02$; pHL, 0.87), SUV$_{P10}$, SUV$_{P90}$, and SUV$_{mean}$ (AUC, 0.70–0.74; $P = 0.003$–0.006; pHL, 0.67–0.70). The combined MLD and SUV$_{P90}$ model generalized in the validation subset and was deemed the final RP$_{Early}$ model (RP$_{Early}$ risk = $1/[1 + e^{(-x)}]$; $x = -6.08 + [0.17 \times MLD] + [1.63 \times SUV_{P90}]$). The final model refitted in the 160 patients indicated improvement over the published MLD-alone model (AUC, 0.77 vs. 0.72; $P = 0.0001$ vs. 0.02; pHL, 0.65 vs. 0.87). **Conclusion:** Patients at risk for RP$_{Early}$ can be detected with high certainty by combining the normal lung's MLD and pretreatment ^{18}F-FDG PET/CT SUV$_{P90}$. This refined model can be used to identify patients at an elevated risk for premature immunotherapy discontinuation due to RP$_{Early}$ and could allow for interventions to improve treatment outcomes.

Key Words: immunotherapy; non–small cell lung cancer; PET/CT; pneumonitis; radiation

The addition of immune checkpoint blockade (ICB) consolidation therapy after concurrent chemoradiation (cCRT) in patients with locally advanced non–small cell lung cancer (NSCLC) has significantly improved survival and represents the current standard of care (1–3). The ICB consolidation therapy is administered intravenously over 1 y and has led to a 3-fold increase in the median progression-free survival and a 10% absolute increase in the 5-y overall survival compared with the prior cCRT alone standard of care (4). However, ICB consolidation therapy has also been found to increase the incidence of symptomatic pneumonitis (1,5,6). Before the use of ICB consolidation, radiation pneumonitis (RP) would result in morbidity but was rarely associated with poor survival. However, the development of RP is increasingly important since it can now lead to the premature discontinuation of ICB consolidation therapy before the planned 1 y and is thereby associated with poorer survival (5,7). Furthermore, early RP (i.e., developing ≤3 mo after completion of cCRT; RP$_{Early}$) has recently been suggested as the most critical toxicity, as it can lead to a markedly insufficient duration of ICB therapy (7,8).

Models to predict the risk of RP have been developed to guide radiation therapy (RT) planning and inform patient counseling, but these models have been derived from patients treated with cCRT alone, and the models further underestimate the rate of RP in patients treated with cCRT and ICB (6). This is largely due to the higher rate of RP with the addition of ICB consolidation (6) but is also due to the limited ability of these models to accurately predict patients with RP even after cCRT alone (9). Given the increased use of ICB consolidation therapy and a growing number of strategies to use immunotherapy agents with cCRT (10), models that accurately estimate the risk of RP in the era of ICB therapy are warranted. In cohorts treated with cCRT alone, pretreatment ^{18}F-FDG PET/CT imaging features are associated with increased RP risk (11). In noncancerous patients, such features have been indicative of pulmonary inflammation and hypothesized to be related to the density and activation of inflammatory immune cells in the lung (12,13).

There are currently no RP risk models specifically developed for RP$_{Early}$. In this study, we hypothesized that incorporating pretreatment ^{18}F-FDG PET/CT features with RT dose would yield risk models able to successfully identify patients with an exacerbated risk of this new critical toxicity, RP$_{Early}$.

MATERIALS AND METHODS

Cohort

In total, 178 patients who had locally advanced NSCLC and were consecutively treated with cCRT and durvalumab between May 2017 and December 2021 at a multisite tertiary cancer center were reviewed, and the 160 patients with pretreatment ^{18}F-FDG PET/CT scans available were included in this study. Patients avoided strenuous exercise for more than 24 h—and fasted for 6 h—before ^{18}F-FDG injection. The required blood sugar level was less than 200 mg/dL. After ^{18}F-FDG administration, the patients were instructed to rest quietly in the injection room. Before the study, the patients were asked to void the urinary bladder. ^{18}F-FDG PET/CT was performed according to institutional guidelines, which are based on the joint European Association of Nuclear Medicine/Society of Nuclear Medicine and Molecular Imaging/European Society for Radiotherapy and Oncology practice recommendations for the use of ^{18}F-FDG PET/CT for external-beam treatment planning in lung cancer (14). The PET/CT scans were acquired in 3 dimensions on a Discovery 690 or 710 PET/CT (GE Healthcare Inc.) (15). Patients were positioned on a flat RT tabletop. Whole-body PET acquisitions commenced about 60 min after administration of approximately 480 MBq of ^{18}F-FDG, at 3 min/bed position. All PET emission data were corrected for attenuation, scatter, and random events and were iteratively reconstructed into a $128 \times 128 \times 47$ matrix (voxel dimensions, $5.47 \times 5.47 \times 3.27$ mm) using an ordered-subset expectation maximization algorithm (2 iterations, 16 subsets) incorporating time-of-flight and point-spread function modeling. A gaussian postprocessing filter of 6.4 mm in full width at half maximum was also applied. Respiratory motion correction was not performed.

Patients were prescribed 60 Gy in 2-Gy fractions concurrent with platinum doublet chemotherapy (6,16). Durvalumab consolidation was initiated at a median of 1.4 mo after cCRT completion (Table 1). All patients had standard follow-ups after treatment, with a history, physical examination, and chest CT scan being obtained every 3 mo for the first 2 y. RP of grade 2 or higher was defined as a patient's having worsening pulmonary symptoms, including dyspnea or cough not attributable to other causes, within 12 mo from the completion of cCRT and having CT-based imaging changes within the irradiated field (5,17). Three RP endpoints were studied: 3 mo after completion of cCRT (RP$_{Early}$), more than 3 mo after completion of cCRT (RP$_{Late}$) (Table 2), and the combination thereof (RP$_{Early+Late}$), which is the definition that has traditionally been used. Patients with clinical and imaging characteristics consistent with RP were retrospectively assessed for their clinical course of RP, and RP grading was based on the Common Terminology Criteria for Adverse Events, version 5.0. This retrospective study was completed under an institutional review board–approved protocol.

Modeling

Applying Published Risk Models to RP$_{Early}$. In our previous work (17), which focused on RP in the thorax after any type of ICB, 3 published RP models were identified and explored: QUANTEC mean lung dose (MLD) alone (18); MLD, age, obstructive lung disease, smoking status, and tumor location (19); and MLD, age, and obstructive lung disease (9). The MLD was extracted for the total normal lung (excluding the tumor) and converted to an equivalent dose in 2-Gy fractions, assuming 3 Gy for the fractionation sensitivity parameter α/β (EQD2$_3$) (18); the other model parameters were extracted from the medical records. Each published model's coefficients were applied to the corresponding parameters (with no refitting). Model suitability was assessed both as calibration via the Hosmer–Lemeshow test (pHL; ideal value, 0.50) and as discrimination via the area under the receiver-operating characteristic curve (AUC; ideal value, 1.00)

and P value (ideal value, 0). Each of the 3 published models was also studied for association with RP$_{Late}$ in addition to RP$_{Early+Late}$.

Integrating ^{18}F-FDG PET/CT Features with Published Risk Models for RP$_{Early}$. To obtain ^{18}F-FDG PET/CT features, the normal lung in the planning CT scan was propagated onto the low-dose CT scan using Plastimatch routines for b-spline–based deformable image registration within the computational environment for RT research (20). All propagated normal-lung contours were quality-controlled to limit the influence of registration uncertainties. The SUV was normalized with respect to the body mass. Since most second-order histogram lung ^{18}F-FDG PET/CT features have previously been found to be nonreproducible across reconstruction algorithms (21–24), only first-order histogram features of the SUV were extracted: 10th percentile of SUV (SUV$_{P10}$), 90th percentile of SUV (SUV$_{P90}$), SUV$_{max}$, SUV$_{mean}$, minimum SUV, and SD. These features adhered to the Image Biomarker Standardization Initiative (25) and were automatically extracted using the radiomics toolbox of the computational environment for RT research (26).

A TRIPOD type 2b model (27) was generated in which the 160-patient cohort was randomly split, but with similar RP$_{Early}$ and RP$_{Late}$ rates, into a 112-patient subset (70%) used to build the model. The remaining 48-patient subset (30%) was used for internal validation of the built model. During model building, each feature was univariately associated with RP$_{Early}$ using logistic regression with bootstrap resampling (repeated over 1,000 samples), and a candidate predictor was indicated by a P value of less than 0.05. The model parameters in the published models that were found to significantly predict RP$_{Early}$ were refitted to the training data, and a new multivariate model was built with the published model parameters and the ^{18}F-FDG PET/CT predictors. Again, the pHL, AUC, and P values were used to assess model suitability but now of the new combined ^{18}F-FDG PET/CT and published model parameters.

RESULTS

Patient Treatment and RP Characteristics

In total, 38 (24%) of the 160 evaluated patients developed RP at a median of 3 mo (range, 1–9 mo) from cCRT completion (Table 1), initiated durvalumab significantly earlier than patients without RP (median, 41 vs. 45 d; $P = 0.03$; Table 1), and were initiated on steroid therapy. Twenty-four (63%) of the 38 patients with RP had resolution or near resolution of RP symptoms 3 mo from onset (Table 2), and of these, 6 (16%) patients were rechallenged with durvalumab, whereas the remaining patients permanently discontinued durvalumab.

Of the 38 patients who experienced RP, 20 (53%) patients did so as RP$_{Early}$ and the remaining 18 (47%) as RP$_{Late}$ (Supplemental Table 1). Among patients with RP$_{Early}$, 10 (50%) remained on steroids 3 mo from symptom onset and the remaining 10 (50%) had resolution or near resolution of RP symptoms. Additionally, 4 (20%) patients with RP$_{Early}$ were rechallenged with durvalumab (Table 2). The appearance of RP on the diagnostic CT scan along with the corresponding treatment planning CT scan to illustrate the RT field is given in Supplemental Figure 1 (supplemental materials are available at http://jnm.snmjournals.org) for 1 representative patient who developed RP$_{Early}$ and 1 representative patient who developed RP$_{Late}$.

Assessment of Published RP Models in Predicting RP$_{Early}$

Among the 3 published models tested, only the QUANTEC MLD-alone model (18) significantly predicted RP$_{Early}$ (AUC, 0.72; $P = 0.02$; pHL, 0.87; Fig. 1A); the other 2 models (9,19) did not (AUC, 0.62, 0.62; $P = 0.10$, 0.57). Refitting the MLD model

TABLE 1
Patient Characteristics

Characteristic	No RP ($n = 122$)	RP ($n = 38$)	P*
Age (y)	67 (49–84)	73 (45–86)	0.10
Sex			
Female	48 (39)	17 (45)	0.56
Male	74 (61)	21 (55)	
Smoking history			
Ever	119 (98)	35 (92)	0.13
During RT	13 (11)	0 (0)	0.04
Performance status			
ECOG 0	65 (53)	19 (50)	
ECOG 1	57 (47)	19 (50)	0.73
AJCC eighth overall stage			
IIIA	31 (25)	10 (26)	0.20
IIIB	74 (61)	16 (42)	
IIIC	17 (14)	12 (32)	
Diagnosed lung disease			
Yes	34 (28)	33 (87)	0.18
COPD	33 (27)	15 (39)	
Asthma	1 (1)	2 (5)	
Diabetes mellitus	27 (22)	9 (24)	0.84
Histology			
Adenocarcinoma	68 (56)	26 (68)	0.14
Squamous cell	41 (34)	11 (29)	
Other	13 (11)	1 (3)	
PDL1 expression			
<1%	39 (32)	13 (34)	0.83
≥1%-49	26 (21)	8 (21)	
≥50%	31 (25)	11 (29)	
Unknown	26 (21)	6 (16)	
Chemotherapy regimen			
Carboplatin/paclitaxel	56 (46)	15 (39)	0.61
Carboplatin/pemetrexed	32 (26)	12 (32)	
Cisplatin/pemetrexed	22 (18)	7 (18)	
Cisplatin/etoposide	10 (8)	4 (11)	
Other	2 (2)	—	
Days from cCRT end to Durvalumab start	45 (10–234)	41 (13–82)	0.03

*Wilcoxon rank-sum test comparing characteristics between patients with and without RP.

ECOG = Eastern Cooperative Oncology Group; AJCC = American Joint Committee on Cancer; COPD = chronic obstructive pulmonary disease; PDL1 = programmed cell death ligand 1.

Qualitative data are number and percentage; continuous data are median and range.

improved calibration (pHL, 0.65 vs. 0.87). At the National Comprehensive Cancer Network, MLD of 20 Gy or less (MLD $EQD2_3$ ≤ 15 Gy), the predicted risk of RP_{Early} was 20%. To explore the feasibility of reducing MLD beyond this guideline, 9 of 20 patients with RP_{Early} were randomly selected for replanning of their RTs. Three treatment planners specializing in thoracic cancers each replanned 3 patients intending to maximally reduce MLD without compromising any other clinical treatment planning criteria. The MLD could be further reduced in all patients and to a median of 12 $EQD2_3$ Gy (range, 8–15 Gy in $EQD2_3$), compared with the original 13 $EQD2_3$ Gy (range, 9–16 $EQD2_3$ Gy), with individual differences ranging from 0.2 to 2.8 $EQD2_3$ Gy. This MLD reduction resulted in a 1%–6% decrease in predicted RP_{Early} (Fig. 2).

TABLE 2
Data for 38 Patients in Whom RP Developed

cCRT end (mo)	Durvalumab start (mo)	CTCAE grade	RP treatment course	Persistent RP symptoms at 3 mo	Rechallenged with durvalumab
1.3	0.8	3	Hospitalized, oxygen, steroid taper	No	No
1.4	0.1	2	Steroid taper and antibiotics	No	Yes
1.5	0.1	3	Hospitalized, oxygen, steroid taper	Yes, remains on steroids	No
1.6	0.4	2	Steroid taper	Yes, remains on steroids	No
1.7	1.0	3	Hospitalized, oxygen, steroid taper	No	No
2.0	0.3	2	Steroid taper and antibiotics	Yes, remains on steroids	No
2.2	1.1	3	Hospitalized, oxygen, steroid taper	Yes, remains on steroids	No
2.2	1.8	2	Steroid taper and antibiotics	No	Yes
2.3	0.5	2	Steroid taper	No	No
2.3	0.9	2	Steroid taper	No	No
2.5	0.9	2	Steroid taper and antibiotics	No	No
2.5	1.0	2	Steroid taper	Yes, remains on steroids	No
2.7	1.3	3	Hospitalized, oxygen, steroid taper	Yes, remains on steroids	No
3.0	2.1	3	Hospitalized, steroid taper	Yes, remain on steroids	No
3.2	2.5	3	Steroid taper and antibiotics	Yes, remains on steroids, in pulmonary rehab	No
3.3	1.6	2	Steroid taper and antibiotics	Yes, remains on steroids	No
3.3	2.4	2	Steroid taper and antibiotics	No	No
3.3	2.6	2	Steroid taper and antibiotics	Yes, remains on steroids	Yes
3.4	2.8	2	Steroid taper and antibiotics	No	No
3.5	2.8	3	Steroid taper, supplemental oxygen	No	No
3.7	1.9	2	Steroid taper	No	No
3.8	2.3	2	Steroid taper	No	Yes
3.8	2.5	3	Hospitalized, oxygen, steroid taper	Yes, remains on steroids	No
3.9	1.5	3	Hospitalized, oxygen, steroid taper	No	No
3.9	2.3	3	Hospitalized, oxygen, steroid taper	No	No
4.5	3.0	2	Steroid taper	Yes, remains on steroids	No
4.5	3.9	3	Hospitalized, oxygen, steroid taper	Yes, remains on steroids and oxygen	No
4.8	3.0	2	Steroid taper	No	Yes
5.7	4.8	2	Steroid taper	No	No
5.9	4.5	2	Steroid taper and antibiotics	No	No
5.9	4.6	2	Steroid taper	No	No
6.5	5.3	3	Hospitalized, oxygen, steroid taper	Yes, remains on steroids	No
6.8	4.9	2	Steroid taper	No	No
8.0	6.4	2	Steroid taper and antibiotics	No	No
8.4	7.8	2	Steroid taper	No	No
8.7	6.0	2	Steroid taper	No	No
9.0	8.1	2	Steroid taper	No	No

———
CTCAE = Common Terminology Criteria for Adverse Events.

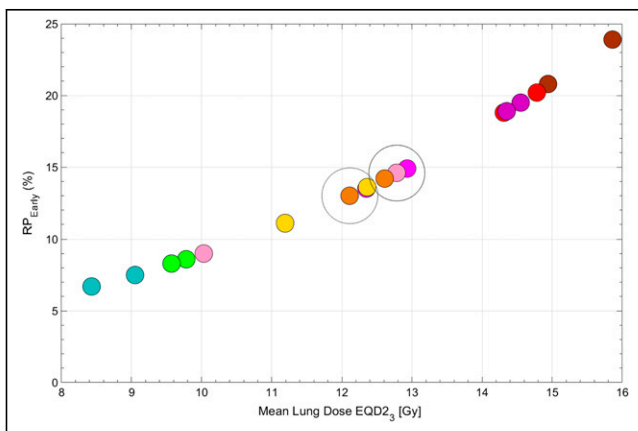**Improved Ability to Correctly Identify RP_Early by Integrating ^{18}F-FDG PET/CT with MLD**

Among all patients, the median SUV$_{mean}$ and SUV$_{max}$ were 0.65 (range, 0.03–1.9) and 10 (range, 0.09–27), respectively. With similar magnitudes of association, SUV$_{mean}$, SUV$_{P10}$, and SUV$_{P90}$

significantly predicted RP$_{Early}$ (AUC, 0.65–0.66; P = 0.003–0.006; pHL, 0.67–0.70). These 3 ^{18}F-FDG PET/CT features were all strongly intercorrelated (Spearman's rho = 0.95). Therefore, bivariate models between MLD and each of these features were built. All bivariate models significantly predicted RP$_{Early}$ in the
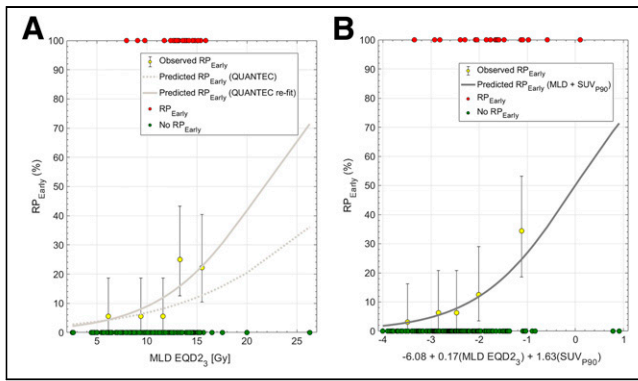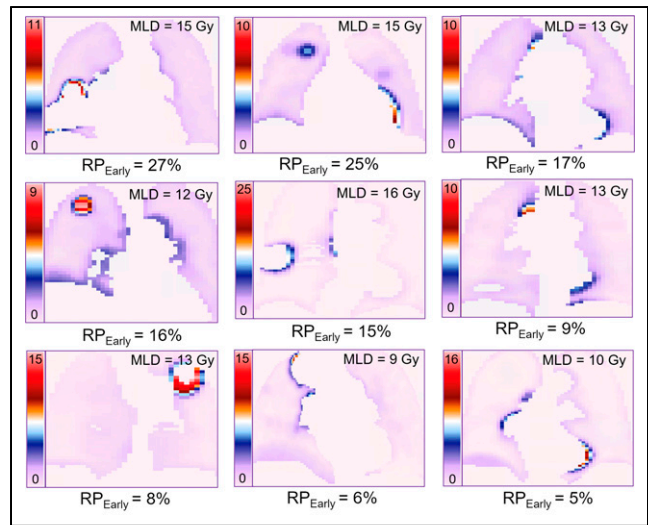
FIGURE 1. (A) Dose–response curve for QUANTEC's MLD model (*18*) (dotted line) applied to RP$_{Early}$ and refitted MLD model for RP$_{Early}$ (solid line) in 160-patient cohort. Observed data are aggregated in quintiles (yellow; error bars: 95% binomial CIs), in addition to each observation stratified by RP$_{Early}$ status. (B) Predicted dose–response curve combining MLD with SUV$_{P90}$ in 160-patient cohort; observed data are aggregated as quintiles (yellow; error bars: 95% binomial CIs), in addition to each observation stratified by RP$_{Early}$ status.

FIGURE 3. Midcoronal slices of highest SUV$_{P90}$ voxelwise distribution maps for 9-patient subset that developed RP$_{Early}$ and were randomly selected for MLD-sparing replanning. MLD EQD2$_3$ is inserted for each patient in upper right corner.

derivation subset (AUC, 0.79–0.80; P = 0.0005–0.0008; pHL, 0.61–0.64), whereas only the model including MLD and SUV$_{P90}$ generalized in the internal validation subset (AUC, 0.65, P = 0.03, pHL, 0.96). This model was, therefore, considered final. Thereafter and only to obtain model coefficients, the final model was refitted to the entire cohort (AUC, 0.77, P = 0.0001, pHL, 0.65; Fig. 2); the risk of RP$_{Early}$ is given by the following logistic function equation: RP$_{Early}$ risk = $1/[1+e^{(-x)}]$; x = −6.08 + [0.17 × MLD] + [1.63 × SUV$_{P90}$]. In the riskiest model quintile, MLD and SUV$_{P90}$ were 15 Gy and 1.51 (Fig. 1B: the rightmost bin), whereas in the least risky quintile, they were 6.7 Gy and 0.89 (Fig. 1B: the leftmost bin). The median SUV$_{P90}$ among patients with RP$_{Early}$ was 1.2 (range, 0.8–2.4), compared with 1.0 (range, 0.05–2.8) for patients without RP$_{Early}$. According to the bivariate MLD and SUV$_{P90}$ model, the risk of RP$_{Early}$ varies for MLDs of similar magnitude. For example, an MLD of 13 Gy is associated with a risk of RP$_{Early}$ varying from 8% to 17% depending on a patient's distribution of SUV$_{P90}$ (Fig. 3).

FIGURE 2. Predicted RP$_{Early}$ based on refitted MLD model alone for random 9-patient subset with RP$_{Early}$ in which replanning was performed. Each color represents each patient, and rightmost circle is MLD from original treatment plan; leftmost circle is MLD from replanning procedure. Population median MLD before and after replanning is denoted by larger circles (right: MLD from original plan; left: MLD after replanning).

No Risk Model Established for RP$_{Late}$

None of the 3 published models (AUC, 0.44–0.52; P = 0.50–0.69; pHL, 0.85–0.99) or any of the 6 ^{18}F-FDG PET/CT features (AUC, 0.55–0.60; P = 0.14–0.58; pHL, 0.71–0.73) predicted RP$_{Late}$. Similarly, no published model significantly predicted RP$_{Early+Late}$ (AUC, 0.55–0.60; P = 0.07–0.98; pHL, 0.99–1.00), but all SUV parameterizations except SUV$_{max}$ were significantly associated with RP$_{Early+Late}$ (AUC, 0.64–0.67; P = 0.006–0.01; pHL, 0.64–0.66), which was likely driven by the stronger association between SUV features and RP$_{Early}$.

DISCUSSION

RP$_{Early}$ in patients with locally advanced NSCLC can lead to the premature discontinuation of life-prolonging ICB consolidation therapy. To date, no risk prediction models have been tested for, or specifically tailored to, RP$_{Early}$. Herein, we present a novel model that combines the MLD with SUV$_{P90}$ of the normal lung from pretreatment ^{18}F-FDG PET/CT, which leads to an improved ability to identify the risk of RP$_{Early}$ over using MLD alone (AUC, 0.72 vs. 0.77). Thus, these results suggest that patients at high risk of RP$_{Early}$ could be identified by assessing the pretreatment SUV$_{P90}$, which could thereby inform patient-specific treatments lowering the MLD to further mitigate RP$_{Early}$. Importantly, the MLD was found to predict RP$_{Early}$ but not RP$_{Late}$, suggesting that the risk of RP$_{Early}$, the most consequential RP in the setting of cCRT and ICB, can be directly mitigated and modified by limiting the MLD of the normal lung.

There is an increased risk of RP in patients who have locally advanced NSCLC treated with cCRT and ICB consolidation therapy compared with cCRT alone (*5,28,29*), with about 25% of patients treated with cCRT and ICB consolidation therapy expected to develop RP. However, only recently have data emerged that early discontinuation of ICB consolidation because of RP is associated with poorer survival and disease control (*6–8*). We have shown that RP models derived from patients treated with cCRT alone widely underestimate the rate of RP in patients treated with cCRT and ICB consolidation (*5*). Although there have been

reports of specific RT dose–volume histogram metrics being associated with the risk of RP in patients treated with ICB consolidation (30,31), these studies have been limited by a small number of patients, leading to inconclusive, conflicting results. Without dose–volume histogram guidelines derived for patients receiving cCRT and ICB consolidation therapy, RT planning and delivery to limit the risk of RP, particularly RP_{Early}, are suboptimal. All 3 published RP models explored here focused on RP prior to the introduction of ICB consolidation (9,18,19). Interestingly, the QUANTEC MLD model (18) was found to be associated with RP_{Early} (AUC, 0.72; $P = 0.04$). The model (19) that in addition to MLD included age, chemotherapy, obstructive lung disease, smoking status, and tumor location did not predict RP_{Early} (AUC, 0.62; $P = 0.57$), and neither did the model (9) that included MLD, age, and obstructive lung disease (AUC, 0.62; $P = 0.10$). Taken together, the inability of published models that include patient characteristics to predict RP_{Early} in patients treated with cCRT and ICB consolidation therapy motivates the need to identify other relevant characteristics to improve the ability to accurately capture RP_{Early}. After thorough model building, the final model generated here that combined SUV_{P90} with MLD had an improved ability to predict RP_{Early} over using MLD alone.

The normal-lung SUV from ^{18}F-FDG PET/CT has previously been found to be elevated among patients with chronic obstructive pulmonary disorder (32) and to be associated with inflammation in acute lung injury (13). The underlying mechanisms of a high SUV in the normal lung have been hypothesized to be attributed to increased density and baseline activation of inflammatory immune cells, as their activation is characterized by increased glucose utilization leading to an increased SUV. Since RP is a consequence of radiation injury and is characterized by increased infiltration of inflammatory cells (33), baseline SUV_{P90} could be an estimate of the degree of pretreatment lung inflammation and, therefore, possibly associated with increased susceptibility toward RP. In this study, we demonstrated that our RP_{Early} model can allow for patient-specific thoracic RT planning to minimize RP_{Early} and ICB discontinuation. Depending on the patient-specific pretreatment SUV_{P90}, the same MLD is associated with a wide risk range of RP_{Early}. In addition, this study indicated that MLD can be further optimized by replanning the RT, which we did for a random 9-patient subset: We demonstrated that the original MLD could be reduced in all patients by 0.2–2.8 $EQD2_3$ Gy and from a median of 13 $EQD2_3$ Gy (range, 9–16 $EQD2_3$ Gy) to a median of 12 $EQD2_3$ Gy (range, 8–15 $EQD2_3$ Gy). This resulted in an RP_{Early} predicted risk reduction of 1%–6% and from a median of 15% (range, 8%–24%) based on the original MLD to 13% (range, 7%–21%) based on the replanned MLD. Reducing the rate of RP_{Early} beyond this would likely require more conformal treatment modalities including particle therapy.

This study provided critical information to guide RT planning and potential risk stratification for patients treated with cCRT and ICB consolidation and further highlighted ideal multidisciplinary expertise and management to optimize lung cancer care (34). Although this was a large study including 160 patients across a multiple-site center, the study had limitations such as a retrospective design based on patients with stage IIIA–IIIC locally advanced NSCLC, and no external validation was performed. These aspects encourage the need for rigorous validation (9) to assess model generalizability and thereby model applicability in other thoracic cohorts presenting with different disease, imaging, patient, and treatment characteristics.

CONCLUSION

Our findings demonstrate that in patients treated with cCRT and ICB consolidation, the RT dose to the normal lungs is strongly associated with the risk of RP_{Early}, the most consequential RP that is associated with poorer survival. Furthermore, we generated a risk model for RP_{Early} based on the upper end of SUV (SUV_{P90}) of the normal lung from pretreatment ^{18}F-FDG PET/CT together with the associated MLD. This model identifies the risk of RP_{Early} with higher accuracy than using MLD alone and could be used to enable patient-specific thoracic RTs specifically tailored to identify and mitigate the risk of RP_{Early} in the context of cCRT and ICB therapies. Such an approach would be anticipated to improve treatment tolerability and, thereby, decrease the likelihood of discontinuing ICB therapies and ultimately prolong survival.

DISCLOSURE

KEY POINTS

QUESTION: Does incorporating pretreatment ^{18}F-FDG PET/CT features with RT dose yield models that would successfully identify patients with an exacerbated risk of RP_{Early}?

PERTINENT FINDINGS: A model was derived that combines the MLD of the normal lung with the SUV_{P90} of the normal lung. The model provided an improved ability to identify RP_{Early} risk over MLD alone.

IMPLICATIONS FOR PATIENT CARE: Incorporating pretreatment SUV_{P90} into clinical practice would enable the delivery of patient-specific RP_{Early} respecting RTs.

REFERENCES

1. Antonia SJ, Villegas A, Daniel D, et al. Durvalumab after chemoradiotherapy in stage III non–small-cell lung cancer. *N Engl J Med.* 2017;377:1919–1929.
2. Antonia SJ, Villegas A, Daniel D, et al. Overall survival with durvalumab after chemoradiotherapy in stage III NSCLC. *N Engl J Med.* 2018;379:2342–2350.
3. Faivre-Finn C, Vicente D, Kurata T, et al. Four-year survival with durvalumab after chemoradiotherapy in stage III NSCLC: an update from the PACIFIC trial. *J Thorac Oncol.* 2021;16:860–867.
4. Spigel DR, Faivre-Finn C, Gray JE, et al. Five-year survival outcomes from the PACIFIC trial: durvalumab after chemoradiotherapy in stage III non-small cell lung cancer. *J Clin Oncol.* 2022;40:1301–1311.
5. Shaverdian N, Thor M, Shepherd AF, et al. Radiation pneumonitis in lung cancer patients treated with chemoradiation plus durvalumab. *Cancer Med.* 2020;9:4622–4631.
6. Shaverdian N, Offin M, Shepherd AF, et al. Association between the early discontinuation of durvalumab and poor survival in patients with stage III NSCLC. *JTO Clin Res Rep.* 2021;2:100197.
7. Xu T, Wu L, Gandhi S, et al. Treatment-related pulmonary events induced by chemoradiation and durvalumab affect survival in locally advanced non-small cell lung cancer. *Radiother Oncol.* 2022;176:149–156.
8. Alessi JV, Ricciuti B, Wang X, et al. Impact of TMB/PD-L1 expression and pneumonitis on chemoradiation and durvalumab response in stage III NSCLC. *Nat Commun.* 2023;14:4238.
9. Thor M, Deasy J, Iyer A, et al. Toward personalized dose-prescription in locally advanced non-small cell lung cancer: validation of published normal tissue complication probability models. *Radiother Oncol.* 2019;138:45–51.
10. Remon J, Levy A, Singh P, Hendriks LEL, Aldea M, Arrieta O. Current challenges of unresectable stage III NSCLC: are we ready to break the glass ceiling of the PACIFIC trial? *Ther Adv Med Oncol.* 2022;14:17588359221113268.

11. Castillo R, Pham N, Ansari S, et al. Pre-radiotherapy PDG PRT predicts radiation pneumonitis in lung cancer. *Radiat Oncol.* 2014;9:74.

12. Vass L, Fisk M, Cheriyan J, et al. Quantitative ^{18}F-fluorodeoxyglucose positron emission tomography/computed tomography to assess pulmonary inflammation in COPD. *ERJ Open Res.* 2021;7:00699–02020.

13. Jones HA, Marsino PS, Shakur BH, Morrell NW. In vivo assessment of lung inflammatory cell activity in patients with COPD and asthma. *Eur Respir J.* 2003; 21:567–573.

14. Vaz SC, Adam JA, Delgado Bolton RC, et al. Joint EANM/SNMMI/ESTRO practice recommendations for the use of 2-[18F]FDG PET/CT external beam radiation planning in lung cancer V1.0. *Eur J Nucl Med Mol Imaging.* 2022;49: 1386–1406.

15. Grkovski M, Schwartz J, Rimner A, et al. Reproducibility of ^{18}F-fluoromisonidazole intratumor distribution in non-small cell lung cancer. *EJNMMI Res.* 2016;6:79.

16. Thor M, Shepherd AF, Preeshagul I, et al. Pre-treatment immune status predicts disease control in NSCLCs treated with chemoradiation and durvalumab. *Radiother Oncol.* 2022;167:158–164.

17. Shaverdian N, Beattie J, Thor M, et al. Safety of thoracic radiotherapy in patients with prior immune-related adverse events from immune checkpoint inhibitors. *Ann Oncol.* 2020;31:1719–1724.

18. Marks LB, Bentzen SM, Deasy JO, et al. Radiation dose–volume effects in the lung. *Int J Radiat Oncol Biol Phys.* 2010;76(suppl):S70–S76.

19. Appelt AL, Vogelius IR, Farr KP, Khalil AA, Bentzen SM. Towards individualized dose constraints: adjusting the QUANTEC radiation pneumonitis model for clinical risk factors. *Acta Oncol.* 2014;53:605–612.

20. Deasy JO, Blanco AI, Clark VH. CERR: a computational environment for radiotherapy research. *Med Phys.* 2003;30:979–985.

21. Orlhac F, Soussan M, Maisonobe JA, Garcia CA, Vanderlinden B, Buvat I. Tumor texture analysis in ^{18}F-FDG PET: relationships between texture parameters, histogram indices, standardized uptake values, metabolic volumes, and total lesion glycolysis. *J Nucl Med.* 2014;55:414–422.

22. van Velden FHP, Kramer GM, Frings V, et al. Repeatability of radiomic features in non-small-cell lung cancer [18F]FDG-PET/CT studies: impact of reconstruction and delineation. *Mol Imaging Biol.* 2016;18:788–795.

23. Yan J, Chu-Shern JL, Loi HY, et al. Impact of image reconstruction settings on texture features in ^{18}F-FDG PET. *J Nucl Med.* 2015;56:1667–1673.

24. Lasnon C, Majdoub M, Lavigne B, et al. ^{18}F-FDG PET/CT heterogeneity quantification through textural features in the era of harmonization programs: a focus on lung cancer. *Eur J Nucl Med Mol Imaging.* 2016;43:2324–2335.

25. Zwanenburg A, Vallières M, Abdalah MA, et al. The Image Biomarker Standardization Initiative: standardized quantitative radiomics for high-throughput image-based phenotyping. *Radiology.* 2020;295:328–338.

26. Apte AP, Iyer A, Crispin-Ortuzar M, et al. Technical note: extension of CERR for computational radiomics: a comprehensive MATLAB platform for reproducible radiomics research. *Med Phys.* 2018;45:3713–3720.

27. Moons KGM, Altman DG, Reitsma JB, et al. Transparent reporting of a multivariable prediction model for individual prognosis or diagnosis (TRIPOD): explanation and elaboration. *Ann Intern Med.* 2015;162:W1-73.

28. Gao RW, Day CN, Yu NY, et al. Dosimetric predictors of pneumonitis in locally advanced non-small cell lung cancer patients treated with chemoradiation followed by durvalumab. *Lung Cancer.* 2022;170:58–64.

29. Hassanzadeh C, Sita T, Savoor R, et al. Implications of pneumonitis after chemoradiation and durvalumab for locally advanced non-small cell lung cancer. *J Thorac Dis.* 2020;12:6690–6700.

30. Mayahara H, Uehara K, Harada A, et al. Predicting factors of symptomatic radiation pneumonitis induced by durvalumab following concurrent chemoradiotherapy in locally advanced non-small cell lung cancer. *Radiat Oncol.* 2022; 17:7.

31. Diamond BH, Belani N, Masel R, et al. Predictors of pneumonitis in patients with locally advanced non-small cell lung cancer treated with definitive chemoradiation followed by consolidative durvalumab. *Adv Radiat Oncol.* 2022;8:101130.

32. de Prost N, Tucci MR, Vidal Melo MF. Assessment of lung inflammation with ^{18}F-FDG PET during acute lung injury. *AJR.* 2010;195:292–300.

33. Kainthola A, Haritwal T, Tiwari M, et al. Immunological aspect of radiation-induced pneumonitis, current treatment strategies, and future prospects. *Front Immunol.* 2017;8:506.

34. Berghmans T, Lievens Y, Aapro M, et al. European Cancer Organisation Essential Requirements for Quality Cancer Care (ERQCC): lung cancer. *Lung Cancer.* 2020;150:221–239.